Applied Catalysis B: Environmental 166–167 (2015) 432–444

Contents lists available at ScienceDirect

Applied Catalysis B: Environmental

journal homepage: www.elsevier.com/locate/apcatb

Synthesis, characterization and study of lanthanum phosphates as light alcohols dehydration catalysts

T.T.N. Nguyen[a], V. Ruaux[b], L. Massin[a], C. Lorentz[a], P. Afanasiev[a], F. Maugé[b], V. Bellière-Baca[c], P. Rey[c], J.M.M. Millet[a,*]

[a] Institut de Recherches sur la Catalyse et l'Environnement de Lyon, IRCELYON, UMR5256 CNRS-Université Claude Bernard Lyon 1, 2 avenue A. Einstein, F-69626 Villeurbanne Cedex, France
[b] Laboratoire Catalyse et Spectrochimie EnsiCaen CNRS-Unicaen, 6 boulevard Maréchal Juin, 14050 Caen Cedex, France
[c] Adisseo France SAS, Antony Parc 2, 10 Place du Général de Gaulle, F-92160 Antony, France

ARTICLE INFO

Article history:
Received 17 July 2014
Received in revised form
27 November 2014
Accepted 1 December 2014
Available online 3 December 2014

Keywords:
Alcohol dehydration
Acid catalysts
Lanthanum phosphates catalysts
Alkenes

ABSTRACT

Four preparation methods have been developed for the synthesis of lanthanum orthophosphate catalysts, which are shown to be active and selective catalysts for the dehydration of light alcohols (C_2 to C_4). Their crystallinity, surface area, surface composition and acid–base properties appear to differ according to the preparation method used. The most important parameter influencing their catalytic properties appears to be their surface composition since this has a direct influence on their surface acidity. All of the solids presented weak and moderately strong Brønsted and Lewis acid sites, and only weak basic sites in low quantities. These acid–base properties resulted in the prevalence of an E_1-type mechanism for 1-butanol dehydration. Brønsted acid sites, which appear as the most efficient sites, are associated with the presence of an excess of phosphorus at their surface and from spectroscopic data this is attributed to $(H_2PO_4)^{-3+n}$ ($n = 1$ or 2) species from spectroscopic data. The prevalence of these species and their optimum surface distribution make them extraordinarily efficient and ultra-selective for the dehydration of several alcohols.

Published by Elsevier B.V.

1. Introduction

Nowadays, light alkenes are produced mainly from the thermal cracking of liquefied petroleum gas or naphtha [1]. However, the declining availability of raw fossil materials, which has led to irregular global distribution patterns and higher prices, has encouraged the chemical industry to consider a progressive changeover to the use of renewable feedstock such as light alcohols, which start to be produced in large quantities and for which competitive dehydration processes are available. Furthermore, these new processes have many additional advantages, in particular their reduced CO_2 emissions, low production costs, and low energy requirements.

There are many solid acid catalysts, which are efficient in catalyzing the dehydration of ethanol. These catalysts include supported phosphoric acid, alumina, silica-alumina and zeolites [2–6]. Although supported phosphoric acid was initially used as an industrial catalyst, alumina and silica-alumina took over as a consequence of their higher productivity and stability. They nevertheless require a high reaction temperature (430–450 °C) and are less efficient when bio-ethanol solutions containing a large quantity of water are used as a reactant. For these reasons, zeolite-based catalysts such as HZSM-5 were developed [4,5], allowing the reaction temperature to be lowered (300 °C) with no substantial loss in their catalytic properties (95% ethylene and 98% ethanol conversion in the case of HZSM-5). SAPO catalysts such as SAPO-34 have also been successfully used [6]. However, when the dehydration of alcohols over solid catalysts occurs on mainly acid sites, the strong acidity and non-uniform distribution of these sites leads to undesirable by-products and significant coking. The acidity of HZSM-5 has been modified by doping it with phosphorous [7,8] or a rare earth metal (lanthanum) [9–11], and that of SAPO-34 has been modified by Ni substitution [6], thus leading to the elimination of strong acid sites, an increase in the number of moderately strong or weak acid sites, and an improvement in the catalysts' properties. Nevertheless, a temperature of 300 °C was needed to enhance the ethanol conversion and ethylene selectivity, to improve the catalysts' anti-coking ability, and to achieve a low weight hourly space velocity (WHSV = 2.0 h^{-1}).

Recently new, less conventional catalysts have been proposed, with a high selectivity and activity. These include micro-porous

* Corresponding author. Tel.: +33 472445317; fax: +33 472445399.
E-mail address: jean-marc.millet@ircelyon.univ-lyon1.fr (J.M.M. Millet).

http://dx.doi.org/10.1016/j.apcatb.2014.12.004
0926-3373/Published by Elsevier B.V.

niobium silicates [12], silver salt of tungstophosphoric acid [13] and nano-structured lanthanum phosphates [14,15]. The latter catalysts were prepared with P/La ratios ranging from 0.5 to 2.0, and were active and selective for ethanol dehydration between 200 and 450 °C. The catalytic properties, which are attributed to low or medium acid sites, were found to be influenced by the bulk P-to-La ratio: high P/La ratio (P/La = 2) catalysts had higher ethanol conversion and ethylene selectivity.

In the present study, we report on the use of lanthanum phosphate catalysts for the dehydration of not only ethanol, but also other light alcohols such as 1 and 2-propanol and 1 and 2-butanol. These catalysts are highly efficient, and have been patented for such dehydration reactions as well as several other types of reaction [16]. Four different methods of preparation, described in the literature or developed specifically for this study, were used to synthesize the lanthanum phosphates. The catalytic properties of these phosphates were then compared in terms of their ability to dehydrate ethanol and 1-butanol, and the best candidates were also tested with other light alcohols. Structure–activity relationships were also studied, by characterizing the phosphate catalysts through the use of various techniques including X-ray diffraction (XRD), high resolution transmission electron microscopy (HRTEM), X-ray photoelectron spectroscopy (XPS), temperature-programmed desorption of ammonia and CO_2, and Raman spectroscopy. Special attention was paid to the surface acid–base properties of the catalysts using Fourier transform infrared spectroscopy (FTIR) analysis of pyridine, 2,6-lutidine (2,6-dimethylpyridine) and CO_2 adsorption.

2. Experimental

2.1. Preparation of the lanthanum phosphates

Four methods have been used or developed to prepare the catalysts according to the following procedures:

Method M1: The first method was a two steps method with first the synthesis of a lanthanum gelatinous hydrous oxide slurry and secondly its digestion in an aqueous solution of phosphoric acid [17]. The lanthanum hydrous oxide slurry was prepared by dissolving 6.6 mmol of cetyltrimethylammonium bromide (CTAB) in 100 mL of a 1:1 water-ethanol solution and adding 12 mL of aqueous ammonia (32 wt%). The solution was stirred for 10 min before addition of 2 mol of $La(NO_3)_3{\cdot}6H_2O$. After 2 h under stirring the resulting solid was collected by filtration, washed with distilled water and dried in air. The solid was then digested in an aqueous solution of phosphoric acid (1 mol L^{-1}, 100 mL) for 48 h. The final product was filtered, washed with distilled water, dried in air and calcined at 550 °C for 6 h.

Method M2: The second method consisted in ball milling a mixture of $La(NO_3)_3{\cdot}6H_2O$, Na_2HPO_4 and NaOH [18]. Reagents were weighed out as required by stoichiometry and placed in a mortar and dry milled in air for 3 h by using a pestle. Milled powders were washed with deionized water to eliminate $NaNO_3$ formed as by-product, and dried at 120 °C for 4 h. The solid obtained was calcined at 550 °C for 6 h under air.

Method M3: The third method has been developed for this study. It consisted of two steps with first the preparation of $La(OH)_2NO_3$ and second the topotactic formation of $LaPO_4$ from solid $La(OH)_2NO_3$ and $(NH_4)H_2PO_4$ solution. In a typical synthesis, hydrated lanthanum nitrate was mixed with tenfold molar excess of $NaNO_3$; the mixture was pre-treated under a nitrogen flow at 150 °C for 2 h, then the reaction was carried out at 500 °C for 4 h. After cooling, the resulting $La(OH)_2NO_3$ solid was washed with distilled water and dried at 100 °C in air for 12 h. 3 g of $La(OH)_2NO_3$ and 9 g of $(NH_4)H_2PO_4$ were finally added to 200 mL of distilled water. The solution was then stirred for 48 h and the precipitate was collected by filtration, washed with distilled water and dried in air at 120 °C.

Method M4: This method was based upon the precipitation from lanthanum nitrate hexahydrate and phosphoric acid sol [19]. The sol was gelled in an ammonia atmosphere for 24 h and the gel as obtained was first dried at 50 °C, washed with deionized water and then with octanol three times within a duration of 3 h and dried at 50 °C. The sample was finally calcined at 450 °C. Two other $LaPO_4$ samples respectively named $LaPO_4$-M4-1 and $LaPO_4$-M4-2 have been synthesized using this method adding more orthophosphoric acid. The excess of phosphorus corresponded to P/La of 1.2 and 1.35.

2.2. Characterization of the catalysts

Metal contents of the solids were determined by atomic absorption (ICP) using Activa device (Horiba Jobin Yvon). The specific surface areas (SSA) of the catalysts were calculated by nitrogen physisorption at −196 °C using a Micromeritics ASAP 2020 instrument and the BET method. Prior to measurements, the samples were degassed under vacuum of 10^{-4} Pa for 3 h at 300 °C. Complete isotherms were recorded on the solids pretreated similarly. Powder X-ray diffraction (XRD) patterns were obtained using a Bruker D5005 diffractometer with CuKα radiation (recording conditions: 0.02° (2θ) steps over 10°–80° 2θ angular range with 10 s counting time per step). The unit cells of the phosphate phases were refined using Bruker Topas P program. High-resolution transmission electron microscopy (HRTEM) was done using JEOL 2010 equipment operating at 200 kV with a high-resolution pole piece and an energy-dispersive X-ray spectrometer (EDX; Link Isis, Oxford Instruments). XPS measurements were performed using a Kratos Axis Ultra DLD spectrometer. Spectra of La 3d and 4d, P 2p, O 1s, C 1s (and eventually Na and N 1s when present) levels were measured at 90° (normal angle with respect to the plane of the surface) using a monochromated Al Kα X-ray source with a pass energy of 20 eV. Binding energies were corrected relative to the carbon 1s signal at 284.6 eV. The signal intensities of La 4d, P 2p, O 1s and C 1s were measured using integrated areas under the detected peak. The experimental precision on XPS quantitative measurements was considered to lead to precision on the calculated cationic ratio of 0.1.

Raman spectra were measured on a Jobin-Yvon LabRam Infinity apparatus equipped with a CCD detector operating at liquid nitrogen temperature. A D2 filter was used to protect the catalyst structure from destruction by the laser (wavelength λ = 520 nm). The Raman shift was recorded in the range 200–5500 cm^{-1}. The homogeneity of the samples was evaluated by performing the analysis on at least three different locations for each sample. FTIR spectra of the phosphates were recorded in transmission between 400 and 4000 cm^{-1} on a Vector 22 of Bruker. The samples were prepared as by dilution of about 1–2 mg in 300 mg of KBr.

FTIR spectroscopy has also been used to characterize the acid–base properties of the catalysts by following the spectra of adsorbed probe molecule. This type of study has been conducted using a Nexus 670 FTIR spectrometer equipped with a MCT (Mercury Cadmium Telluride) or DTGS (Deuterated Tri Glycine Sulphate) detector. The samples of phosphates were pressed into self-supporting pellets (20–30 mg, 2.01 cm^2), placed in the cell, and treated at 300 °C in situ under vacuum (10^{-5} Torr) for 1 h. After cooling to 100 °C, they were exposed to vapor of pyridine, 2,6-lutidine (1 Torr at equilibrium) or CO_2 (10 Torr at equilibrium) for 15 min. The spectra (128 scans, resolution of 4 cm^{-1}, range of acquisition: 400–4000 cm^{-1}) were then recorded after evacuation under vacuum (10^{-5} Torr) at 25, 50, 100, 150, 200 and 250 °C for 15 min. Spectral analyses and decompositions were carried using Omnic software. All spectra presented in the paper were normalized to

a disk of 5 mg cm^{-2}. In some case data were also normalized to similar specific surface area.

Temperature-programmed desorption (TPD) of NH_3 and CO_2 have been used to measure the amount of acidic and basic sites and their distribution in strength. The thermo-desorption apparatus was a BELCAT thermo analyzer. 60–80 mg of samples were first treated at 450 °C for 1 h under helium flow (15 mL min^{-1}) and cooled down to the adsorption temperature (100 °C) before exposition to NH_3 (or CO_2) for 30 min. Following, the system was swept by He for 15 min and temperature was programmed to increase to 550 °C with heating rate of 8 °C min^{-1}.

2.3. Catalytic testing

The catalytic performances of the catalysts were determined at atmospheric pressure between 200 and 470 °C in a micro-pilot testing apparatus using a fixed-bed down-flow reactor. Typically, the catalyst was packed into a glass plug-flow micro-reactor and stabilized in the flowing of nitrogen for 1 h. High purity nitrogen was used as a carrier gas and the alcohol was introduced into the carrier gas by an evaporator–saturator system, which was placed in a cryostat. All the pipes were heated to eliminate condensation of alcohol and liquid products. The alcohols and reaction products were analyzed online by gas chromatography. A two-dimensional chromatography also coupled to mass spectroscopy (GC–MS-2D) of SRA instrument equipped a ZB1 column and a VF17 column, has been used to detect traces of by-products when almost 100% selectivity was observed. Calculated carbon balances were higher than 98%. Tests of empty reactor for the dehydration of ethanol, 2-butanol and 1-butanol were carried out at 355 °C with the conversion always lower than 3%. In this case, the dehydration of 2-butanol gave mainly 2-buten and that of 1-butanol mainly 1-butene. Cis and trans 2-butenes ratios were not systematically determined however all the analyses done showed a cis to trans ratio equal to 0.9 ± 0.05. All products were reagent grade and gases from the IRCELYON internal gas distribution system were used without further purification. The catalytic properties of the lanthanum phosphates have been compared to an Al_2O_3 industrial reference catalyst with a specific surface area of 270 m^2 g^{-1}.

3. Results

3.1. Characterization of the catalysis

The physicochemical characteristics of the prepared catalysts are presented in Table 1. The P:La ratios obtained from chemical analysis were slightly higher than the theoretical ones for all the solids except M3. Their specific surface areas were comprised between 110 and 170 m^2 g^{-1}. Although these surface areas were high, the pore volumes of the solids were small, with pore size equal to that of mesopores. No correlation between the surface areas and the pores sizes was found and the latters should be related to the preparation method. The solids prepared using method M4 with different P/La ratios exhibited rather similar specific surface areas. The XRD patterns of the prepared compounds are displayed in Fig. 1. The solids prepared using methods M1 and M4 corresponded to well-crystallized pure phases whereas those prepared using method M2 (mecano-synthesis) and M3 (heated at low temperature) were poorly crystallized. All the patterns corresponded to the $LaPO_4$ Rhabdophane structure type (ICSD 046-1439) except $LaPO_4$-M2, which contained a small amount of Monazite phase. HRTEM study clearly showed that in all the phosphate samples except $LaPO_4$-M2 the particles were made of nanorods or nanowires forming bundles (Fig. 2a). The almost complete absence of preferred growth direction for the M2 sample particles may be a consequence of the preparation protocol by mecano-synthesis. The nanorods have diameter and length respectively ranging from 4 to 13 nm and from 17 to 70 nm (Fig. 2b). No correlation was found with other texture parameters. Morphology was such that surface exposure of (h k 0) planes was maximized and it was difficult to get an image of the nanowires in the [h k 0] direction. On the surface of the (h k 0) planes the structure showed alternatively rare earth cation-oxygen, chains separated from each other by PO_4 whereas in the (0 0 1) plane the structure channels could be clearly evidenced (Fig. 2c and d). These observations were in good agreement with previous studies [20,21]. No restructuration of the surface with the formation of an amorphous layer was observed in any high-resolution images recorded before or after testing. Although all of the preparation

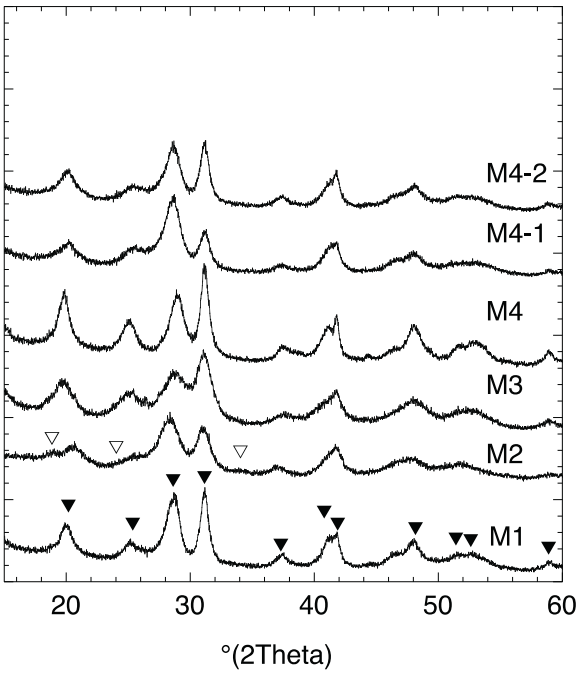

Fig. 1. XRD patterns of lanthanum phosphates with Rhabdophane (ICSD 046-1439 ▼) and Monazite structures (ICSD 035-0731 ▽).

Table 1
Bulk and surface atomic ratios of $LaPO_4$ catalysts calculated from chemical and XPS analyses and results of specific surface areas and pore sizes measurements. SSA: Specific surface area.

Catalyst	P/La atomic ratio		SSA (m^2 g^{-1})	Pore diameter (nm)	Pore volume (cm^3 g^{-1})
	Bulk	Surface			
$LaPO_4$-M1	1.1	1.32	124	8	0.2
$LaPO_4$-M2	1.1	1.23	128	4	0.1
$LaPO_4$-M3	1.2	1.30	112	13	0.3
$LaPO_4$-M4	1.1	1.08	159	14	0.5
$LaPO_4$-M4-1	1.1	1.38	170		
$LaPO_4$-M4-2	1.0	1.41	150		

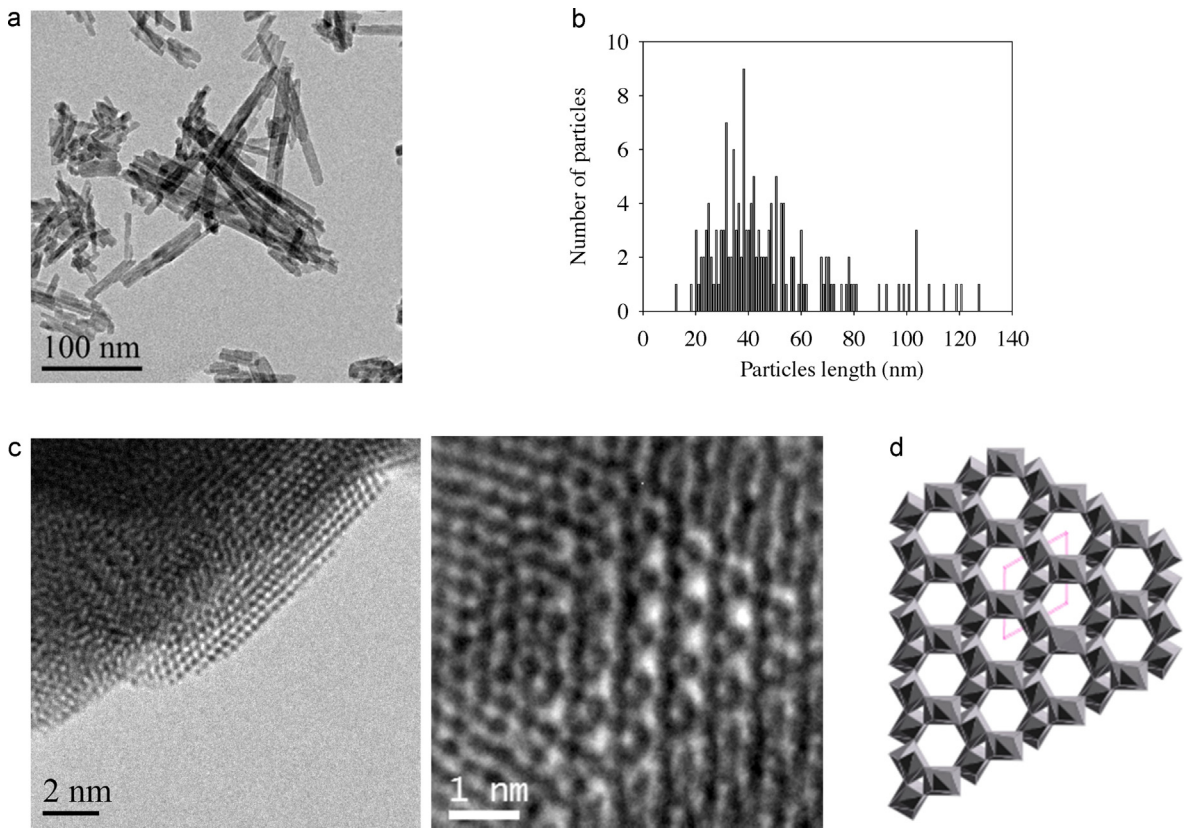

Fig. 2. HRTEM micrographs of as-synthesized hydrated hexagonal $LaPO_4$-M1 (a) with particles length distribution (b). HRTEM micrographs in the [0 0 1] direction (c) and in the [1 1 0] direction (d), with a schematic representation of the structure in the same direction.

protocols were not using stabilizing agents, all of the X-ray diffraction patterns showed the same preferential growth.

The surface composition of the catalysts has been studied by XPS. First, spectra have been recorded over a broad energy range in order to evidence the possible presence of elements other than La, P, O and eventually C at the surface of the lanthanum phosphates. These spectra showed no contamination or doping except for $LaPO_4$-M3 for which small peaks corresponding to N 1s (NH_4^+) and to Ca 3d were detected. In this case the surface composition of Ca and N did not overpass 1%. All binding energies calculated were in good agreement with those published earlier [22,23]. The phosphorus in the four phosphates existed in the form of PO_4 with the same binding energy (133.3 ± 0.1 eV). The La 3d 5/2 and La 3d 3/2 binding energies were in good agreement with those reported elsewhere [24,25]. The P/La ratio varied between 1.08 and 1.40 depending upon the preparation method used and in the case of M4 as a function of the amount of phosphate precursor used for the synthesis (Table 1). These surface ratios were higher than the bulk ones determined by chemical analyses. Such feature is common to almost all phosphates based catalysts and has been reported for iron, titanium and vanadium phosphates [26–28]. A special attention has been given to the analysis of the O 1s peak. Adequate peak fitting could systematically be achieved with two components attributed to O^{2-} (531.0 eV) and OH^- (532.6 eV). The position of the O 1s XPS peak for oxygen-containing carbon species (C—O and O=C—O) is around 531.8 eV and a contribution of these species should not be completely discarded even if C 1s peak was very weak for most of the solids. The calculated relative OH content seemed rather constant (13–18%). However it is difficult to draw conclusions since OH species corresponding either to P—OH or La—OH species cannot be undoubtedly distinguished. The phosphates catalysts have been characterized using Raman spectroscopy. All the spectra were comparable. The general bands attribution is given on Table 2. P—O stretching modes were observed in the 1100–900 cm^{-1} region. Seven or eight phosphate bending modes were observed between 400 and 642 cm^{-1}, the asymmetric ones being over 500 cm^{-1} [22]. Besides the bands corresponding to the Rhabdophane structure two bands at 904-08 and 967-85 cm^{-1} were observed. They have respectively been assigned to the P—OH bond stretching mode of the symmetric P—$(OH)_2$ vibration and to the stretching vibration of the P—O bond in the adsorbed $(H_nPO_4)^{-3+n}$ [29]. Finally a relatively sharp band around 3460 cm^{-1} has been detected and attributed to the La—OH stretching vibration.

The lanthanum phosphates have been characterized by ^{31}P solid-state NMR spectroscopy. All the ^{31}P MAS spectra showed a broad peak with a ^{31}P isotropic chemical shift of about −3.2 ppm. This resonance characterizes the $LaPO_4$ phase with Rhabdophane structure with a single crystallographic P site. Small differences in chemical shift for the various samples were observed and could

Table 2
Frequencies (cm^{-1}) of the main bands of the Raman spectra of the lanthanum orthophosphates with corresponding assignment.

Attribution	(cm^{-1})	Attribution	(cm^{-1})
A_g/B_g lattice	223	P-$(OH)_2$ stretch.	900
$(H_nPO_{4-n})^{-3+n}$	271	$((H_nPO_{4-n})^{-3+n}$ stretch.	967
A_g/B_g lattice	377	$(PO_4)^{3-}$ sym. stretch.	975
O-P-O E-bending	392	$(PO_4)^{3-}$ sym. stretch.	991
O-P-O E-bending	412	$(PO_4)^{3-}$ ass. stretch.	1026
O-P-O E-bending	465	$(PO_4)^{3-}$ ass. stretch.	1055
O-P-O F2-bending	538	$(PO_4^3)^-$ ass. stretch.	1084
O-P-O F2-bending	572	La-OH	3455
O-P-O F2-bending	586	P-$(OH)_2$ stretch.	900
O-P-O F2-bending	620	$((H_nPO_{4-n})^{-3+n}$ stretch.	967

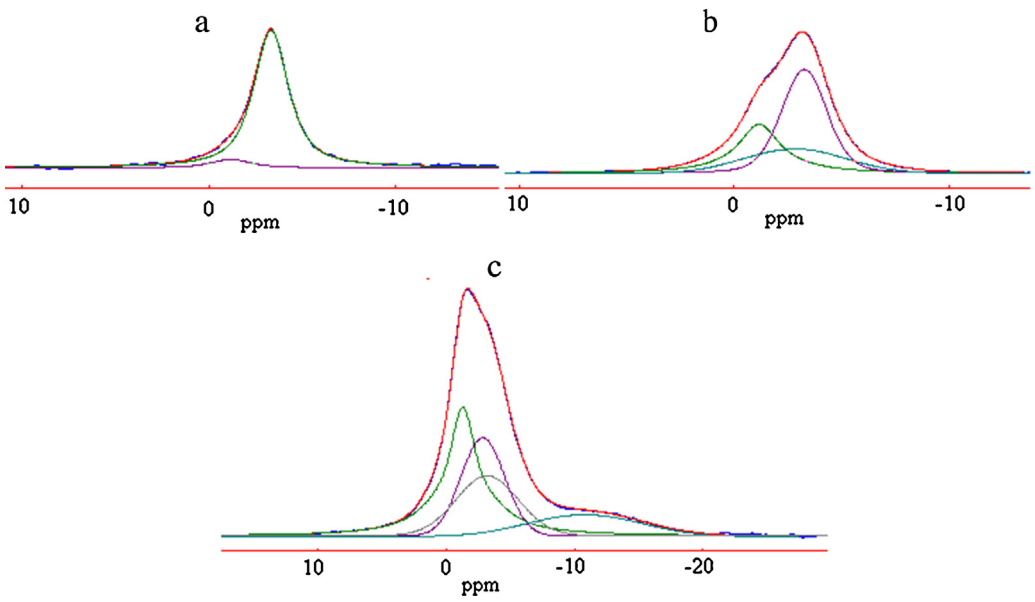

Fig. 3. Fitting of the ^{31}P NMR CP-MAS spectra of the $LaPO_4$-M1 after (a) and before dehydration (b) and of the $H_3PO_4/LaPO_4$-M1 sample. Colored lines are derived from least-square fits. (For interpretation of the references to color in this figure legend, the reader is referred to the web version of the article.)

be explained by different quantities of absorbed water. The ^{1}H-^{31}P cross polarization MAS (CP-MAS) spectrum of the $LaPO_4$ samples allowed the selective observation of $^{31}PO_4$ tetrahedral surrounded by ^{1}H nuclei (Fig. 3). In order to better understand the interaction of PO_4 tetrahedra with water, the $LaPO_4$-M1 sample has been dehydrated at 300 °C for 2 h under vacuum and a new ^{31}P CP-MAS spectrum has been recorded (Fig. 3b). The spectrum of the hydrated sample consisted of three components with chemical shifts at −1.17, −2.83 and −3.19 ppm whereas that of the dehydrated sample consisted of only a strong intense peak at −3.32 ppm with a small shoulder at −1.17 ppm. The −3.32 ppm signal should correspond to PO_4 species in interaction with protons at the surface of the solid. Considering the results of other spectroscopic techniques, this resonance was attributed to $(H_nPO_4)^{-3+n}$ species (n = 1 or 2). Two peaks at around −1.17 and −2.83 ppm were due to the interaction with protons from water molecules. Base on the fact that the interaction with proton leads to shift of NMR signals toward stronger fields, the higher shift could be attributed to $(H_nPO_4)^{-3+n}$ in interaction with water and the lower shift to $(PO_4)^{3-}$ in interaction with water. This attribution fit with the total disappearance of the later peak upon dehydration treatment and with the remaining hydration of the surface hydrogeno-phosphate species, which are more sensitive to rehydration. The results of the fitting are summarized in Table 3. In the ^{31}P CP-MAS spectrum of $LaPO_4$-M2, an additional resonance was detected at 7.6 ppm, which has been assigned in the literature to $(P_2O_7)^{4-}$ interacting with protons [30]. However such species have not been detected by other techniques in this compound. In order to try to ascertain the peak attribution, a sample containing H_3PO_4 supported on $LaPO_4$-M1 has been prepared and characterized by ^{1}H-^{31}P CP-MAS (Fig. 3c) This sample was simply prepared by impregnating $LaPO_4$-M1 with an aqueous solution of H_3PO_4 then dried in air at 120 °C. The same peaks were observed in the spectrum however a new large peak at −10.8 ppm that may be attributed to pyro or polyphosphates species was observed [30] (Table 3).

3.2. Acid–base properties of the lanthanum phosphates catalysts

In order to identify the active and selective sites on the catalysts and to correlate the catalytic properties with the acid–base properties, the lanthanum phosphates have been characterized by adsorption of Pyridine, 2,6-lutidine and CO_2 molecules followed by infrared spectroscopy and temperature-programmed desorption (TPD) of NH_3 and CO_2. Pyridine is a common probe molecule to distinguish Brønsted and Lewis sites. However, it is a weak base with a pK_{BH+} of 5.23 (referred to the usual standard state in water at 25 °C [31]) and is not well adapted to the detection of weak acid sites [32]. In order to study weaker acid sites the adsorption of 2,6-lutidine (pK_{BH+} = 6.75) has been studied. Prior to probe molecules adsorption, the initial FTIR spectrum of the lanthanum phosphates exhibited a broad band at 3670 cm^{-1} corresponding to stretching of O—H vibrations in P—OH groups. In the case of $LaPO_4$-M3, two other peaks at 3546 and 3523 cm^{-1}, which are those of the N—H vibrations of ammonium cations, also detected by other spectroscopic techniques, could be distinguished. Finally all of the spectra presented broad, weak bands in the region 2000–2100 cm^{-1} region that is assigned to P=O vibrations in O=P—OH groups [33].

3.2.1. Pyridine adsorption

Spectra of $LaPO_4$-M1 arising from pyridine adsorption followed by evacuation at different temperatures are shown in Fig. 4. The weak broad shoulder at 1638 cm^{-1}, the weak broad band

Table 3
Results of the fitting of the ^{31}P NMR CP-MAS spectra of the studied catalysts.

Catalysts	$(H_nPO_{4-n})^{-3+n}\cdot nH_2O$ (#1)	$PO_4\cdot nH_2O$ (#2)	$(H_nPO_{4-n})^{-3+n}$ (#3)	Polyphosphate (#4)
$LaPO_4$-M1	−1.2	−2.8	−3.3	–
$LaPO_4$-M2	−1.2	−2.8	−3.3	−7.6
$LaPO_4$-M3	−1.2	−2.6	−3.2	–
$LaPO_4$-M4	−1.3	−2.8	−3.5	–
$H_3PO_4/LaPO_4$-M1	−1.3	−2.9	−3.2	−10.8

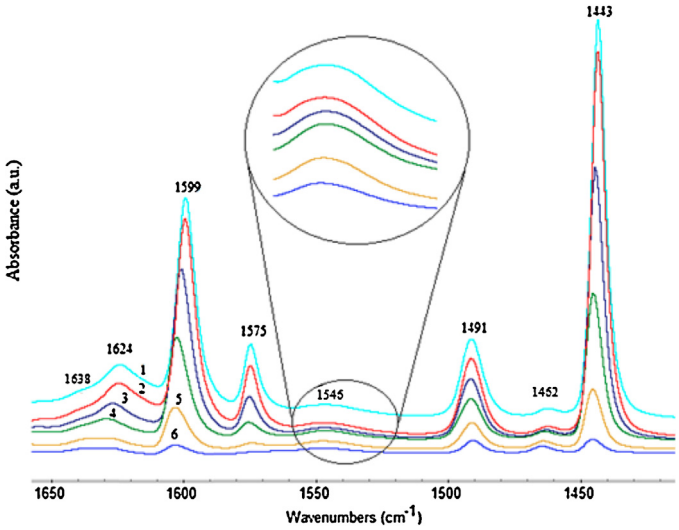

Fig. 4. Infrared spectra of pyridine adsorbed on $LaPO_4$-M1 after desorption under vacuum at: 1: RT; 2: 50 °C; 3: 100 °C; 4: 150 °C; 5: 200 °C; 6: 250 °C.

at 1546 cm^{-1} and the strong band at 1491 cm^{-1} corresponded to vibrations of pyridinium ions formed on Brønsted acid sites [34–37]. Similarly, the broad band at 1624 cm^{-1}, the strong bands at 1443, 1491, 1575 and 1599 cm^{-1} were assigned to the vibrational modes of pyridine coordinated on Lewis acid sites. Some bands are associated to both Brønsted and Lewis acid sites as that around 1491 cm^{-1}. In addition, H-bonded species also contribute to the bands at 1443 and 1599 cm^{-1} [34]. The small band at 1462 cm^{-1} has been assigned to a complex between pyridine and Lewis acid sites [37]. In this complex, pyridine would interact simultaneously with lanthanum cation acting as Lewis acid site and an OH group present nearby. Besides the mentioned bands, bands at 1482 and 1580 cm^{-1} (not shown) were attributed to physisorbed pyridine. These bands disappeared after evacuation under vacuum at ambient temperature (spectrum 1 in Fig. 4). It should be noted that the higher the out-gassing temperature, the higher the wavenumbers of the bands around 1443 and 1624 cm^{-1}. Higher wavenumbers indicate stronger bonding with the surface and hence higher Lewis acid strength. Thus, the shift points out that after high temperature evacuation, pyridine specifically interacts with the strong Lewis acid sites. All these bands were observed for the different lanthanum phosphates samples except $LaPO_4$-M4, which spectrum did not show the bands related to Brønsted acid sites.

The spectra recorded after pyridine desorption at 150 °C for the different samples were comparable. The wavenumbers of the bands corresponding to Lewis acid sites varied in the order M3 > M1 > M2 ~ M4. This pointed out that the Lewis acid strength varies with this ranking. The relative amounts of Brønsted and Lewis sites, expressed as areas under the 1545 cm^{-1} (PyH^+) and 1599 cm^{-1} (PyL) bands, normalized per unit of specific surface area, have been compared at evacuation temperatures (Fig. 5). Concerning the Lewis acid sites, it can be observed that following out-gassing at increasing temperatures, the intensity of the band at 1599 cm^{-1} decreased but could still be detected at 250 °C. This indicates the presence of few significantly strong Lewis acid sites. The same behavior was observed for the number of Brønsted acid sites that decreased slowly with temperature. The number of the strongest Brønsted acid sites were found to vary in the order M3 > M1 > M2 > M4 and for the strongest Lewis acid sites M4 > M2 > M1 > M3. It was observed that the higher was the surface concentration P/La, the greater the number of Brønsted acid sites and the lower was the number of surface Lewis acid sites. This was explained by the fact that Brønsted acid sites are related to the presence of excess of phosphates at the surface ($(H_nPO_4)^{-3+n}$ species). When these species covered the surface less rare earth cations corresponding to Lewis acid sites were accessible.

3.2.2. 2,6-Lutidine adsorption

The FTIR spectra were recorded from 2,6-lutidine adsorbed onto $LaPO_4$-M1, following desorption under vacuum at different temperatures. As in the case of pyridine, after 2,6-lutidine adsorption the initial OH stretching band centered on 3670 cm^{-1} decreases in intensity, and a band of perturbed OH groups appears at 3595 cm^{-1} (not shown). The bands corresponding to the free hydroxyl groups are partially restored after desorption at different temperatures. The adsorption of 2,6-lutidine reveals the presence of both Lewis and Brønsted acid sites. The formation of protonated 2,6-lutidine on Brønsted acid sites is characterized by the bands at 1627 and 1649 cm^{-1} [35,38]. These bands are intense and their intensity does not change significantly after outgassing at temperature up to 50 °C. The spectra have adsorption bands characterizing 2,6-lutidine, associated with Lewis acid sites at 1458, 1477, 1581 and 1608 cm^{-1} [35–38]. H-bonded 2,6-lutidine could also contribute to the bands observed at 1602 and 1581 cm^{-1} [35]. The strength of all of the bands attributed to 2,6-lutidine adsorbed on Lewis and Brønsted acid sites decreases with desorption temperature. This decrease in strength is greater in the case of Lewis acid sites than in the case of Brønsted acid sites. The FTIR spectra of 2,6-lutidine were similar on all of the studied phosphates. Nevertheless, the band intensities were different. The changes in peak intensities at 1608 and 1649 cm^{-1}, corresponding to 2,6-lutidine adsorbed onto Lewis and Brønsted sites respectively, were monitored as a

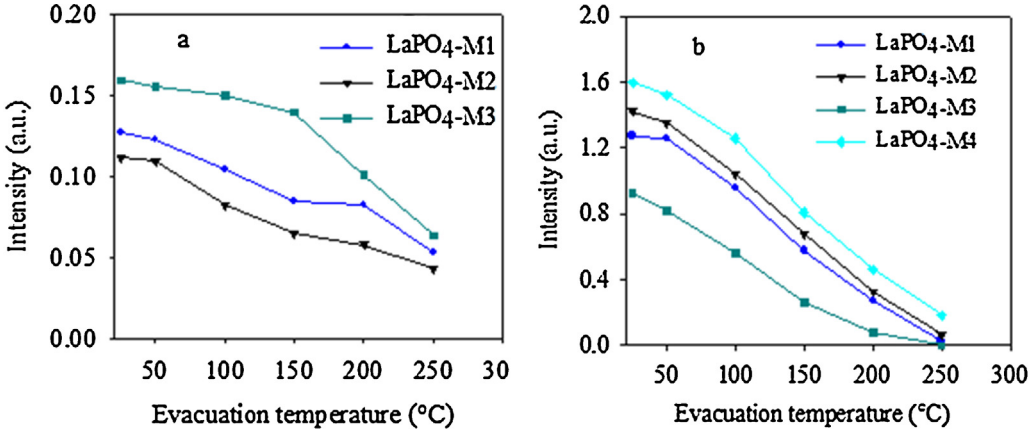

Fig. 5. Normalized intensities of pyridine bands at 1545 cm^{-1} (PyH^+) (a) and at 1599 cm^{-1} (PyL) (b) as a function of evacuation temperature.

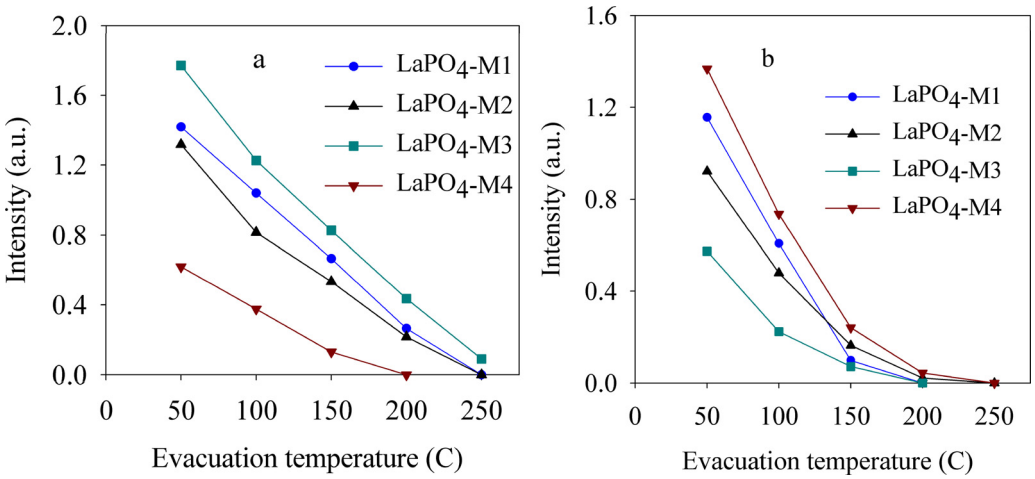

Fig. 6. Normalized intensities of 2,6-lutidine bands at 1649 cm^{-1} (PyH^+) (a) and at 1608 cm^{-1} (PyL) (b) of the $LaPO_4$ catalysts as a function of temperature.

function of outgassing temperature (Fig. 6). For the four different samples, the number of acid sites was ranked in the following order: M3 > M1 ~ M2 > M4 and M4 > M1 > M2 > M3, for the Lewis and Brønsted sites respectively. The Brønsted acid sites could be detected on M3 using 2,6-lutidine, whereas these sites were not detected using pyridine. This indicates the presence of weak Brønsted sites on this sample.

3.2.3. CO_2 adsorption

Spectra of CO_2 adsorbed on lanthanum phosphates were recorded after out-gassing at both room temperature and 100 °C. The intensity of bands was low indicating that the lanthanum phosphate had only a small number of basic sites. Furthermore the intensity of the bands decreased rapidly with increasing temperature showing that these sites were weak. Although the low intensities of the bands made it difficult to analyze the spectra, this was nevertheless attempted. The peaks appearing at approximately 2531 cm^{-1} were attributed to CO_2 adsorption on Lewis acid sites [38]. The bands at 1384 cm^{-1} on $LaPO_4$-M1, 1422 cm^{-1} on $LaPO_4$-M2 and 1441 cm^{-1} on $LaPO_4$-M4, which appeared after evacuation at 25 °C under vacuum but not after out-gassing at higher temperatures could be attributed to the formation of monodentate carbonate. Additionally the bands located at 1620 and 1320–1350 cm^{-1}, which were still apparent after outgassing at 100 °C, could be assigned to surface bicarbonate species [39,40]. Furthermore, a band at approximately 1675 cm^{-1} was observed on $LaPO_4$-M2 and $LaPO_4$-M4, which is consistent with the presence of a bridged carbonate species [34].

3.2.4. Temperature-programmed desorption of NH_3 and CO_2

The NH_3-TPD profiles of the phosphate catalysts are shown in Fig. 7a. In order to analyze these results it was considered that desorption temperatures between 100–150 °C, 150–250 °C, 250–400 °C and 400–550 °C corresponded respectively to very weak, weak, medium strength and strong acid sites respectively. The lanthanum phosphate catalysts are found to contain mainly weak and medium strength acid sites. $LaPO_4$-M3 has the weakest acid sites whereas $LaPO_4$-M1 has the strongest ones. The phosphates prepared using method M1 had the highest number of acid sites, the phosphates prepared using method M2 had the lowest number of weak acid sites, and the phosphates prepared using method M4 had the lowest number of strong acid sites. Moreover, it appeared that NH_3-TPD was able to reveal weak acid sites that could not be revealed by pyridine or 2,6-lutidine adsorption using FTIR. The CO_2-TPD patterns of the different phosphate catalysts are shown in Fig. 7b. Since CO_2 was adsorbed not only on basic sites but also on Lewis acid sites, only the CO_2 desorbed at temperatures above 300 °C was considered. The quantity of CO_2 desorbed under these conditions, was very low, thus confirming the FTIR results. Again, the phosphates prepared using method M1 have the most numerous basic sites and those prepared using M2 had the smallest number of basic sites. From the TPD measurement it was possible to calculate the ratio of acid sites to basic sites, which was consistently higher than 7, and reached 15 in the case of $LaPO_4$-M4.

3.3. Catalytic properties of the lanthanum phosphates catalysts

3.3.1. Dehydration of ethanol

Fig. 8 plots the measured ethanol conversion and product selectivity using the different lanthanum phosphates, as a function of temperature. The main product was ethylene, and the only by-product was diethyl ether. Both ethanol conversion and ethylene selectivity increased with increasing reaction temperature. The $LaPO_4$-M1 and M3 catalysts exhibited the highest catalytic activity for ethanol dehydration, and had comparable selectivities. The other catalysts were markedly less active and selective. Under the chosen catalytic reaction conditions, 100% conversion efficiency was achieved with $LaPO_4$-M1 at 460 °C, although higher temperatures were required for the other catalysts. Traces of ethane were detected on $LaPO_4$-M4 only. The method of preparation clearly has a tremendous influence on the $LaPO_4$ catalysts, in terms of their activity and selectivity. The intrinsic rates of ethanol conversion and the apparent activation energies, were computed for the four $LaPO_4$ catalysts at 285 °C. Although the apparent activation energies appear to be rather similar (121 ± 4 kJ mol^{-1}), the calculated rates vary considerably from one sample to another.

The influence of contact time on the catalytic properties in ethanol dehydration was studied for the case of $LaPO_4$-M1 (Fig. 9). An increase in contact time lowered the reaction temperature at which total conversion and maximum selectivity were obtained. For example, increasing the contact time from 19.8 to 46.0 g_{cata} h mol^{-1} led to a decrease in this temperature from 460 down to 360 °C.

3.3.2. Dehydration of other primary and secondary alcohols

The four lanthanum phosphates catalysts were tested with 1-butanol and isobutanol, and the $LaPO_4$-M1 catalyst was specifically tested with 2-butanol and 1-and 2-propanol. Firstly, all of these catalysts were tested at different temperatures for the dehydration of 1-butanol, using an approach similar to that used for ethanol dehydration. The results shown in Fig. 10a and b, again confirm that these catalysts have significantly different behaviors. $LaPO_4$-M1

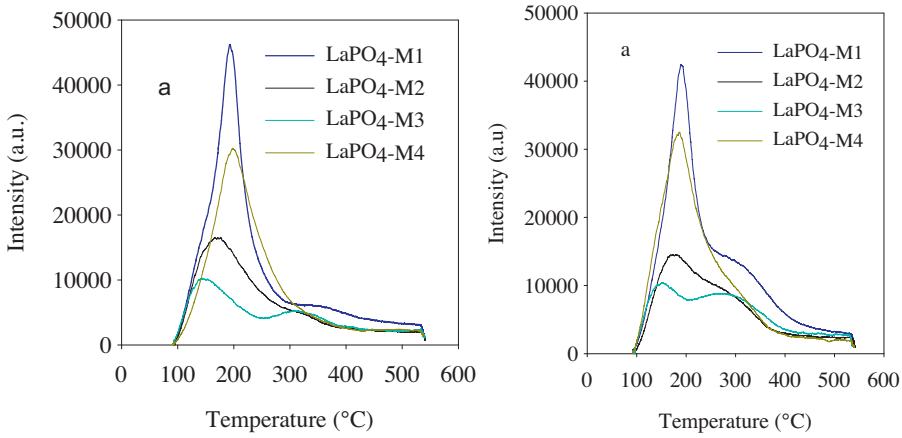

Fig. 7. NH_3-TPD (a) and CO_2-TPD (b) patterns of the $LaPO_4$ catalysts.

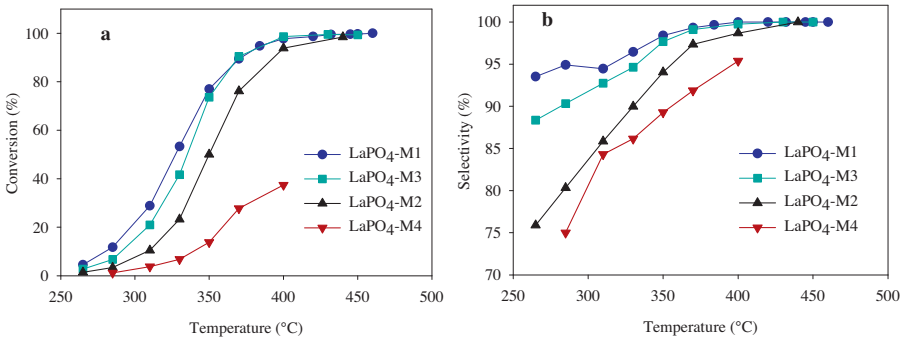

Fig. 8. Evolution of ethanol conversion and products selectivity as a function of temperature on the different lanthanum phosphates. Testing conditions: m_{cata}: 50 mg, W/F = 19.8 g_{cata} h mol^{-1}, N_2: 60 mL min^{-1}.

and M3 are the most active. The opposite trend is observed for the selectivity of 1-butene and 2-butene, i.e. 1-butene is favored at low temperatures (low conversion) whereas 2-butene is favored at high temperatures (high conversion). $LaPO_4$-M1, M2 and M3 exhibit similar selectivities to 2-butene, whereas $LaPO_4$-M4 is much less selective. In addition to the butenes, traces of dibutyl ether (<0.1%) were detected at low temperatures (<280 °C), and traces of ethylene were detected at higher temperatures. Trace quantities of propylene were also detected, when the $LaPO_4$-M4 catalyst was used.

The catalysts were also tested for their isobutanol dehydration properties (Fig. 10c and d). Their ranking in terms of activity is: M1 > M3 > M2 > M4, which is similar to that observed for 1-butanol. Although the main product is systematically isobutene, its selectivity decreases continuously at the advantage of the selectivity to 2-butene. The ranking of these phosphates in terms of selectivity at total conversion was similar to that found for their activity. Like for 1-butanol the reaction products distribution is in favor of a E_1 type mechanism.

Finally, $LaPO_4$-M1 was tested for 2-butanol and 1- and 2-propanol dehydration. The tests were carried out with the same alcohol partial pressure as in the case of ethanol dehydration, in order to use similar contact times (Table 4). In the case of 2-butanol, total conversion was reached at 320 °C and the selectivity to 2- and 1-butene were respectively 74% and 26%. For 1- and 2-propanol dehydration total conversion was achieved at 420 and 300 °C respectively. This catalyst's selectivity to propene never reached 100% since traces or small amounts of propane were systematically observed.

In many cases, nearly 100% selectivity to the alkene was observed at total conversion. As these results were quite surprising,

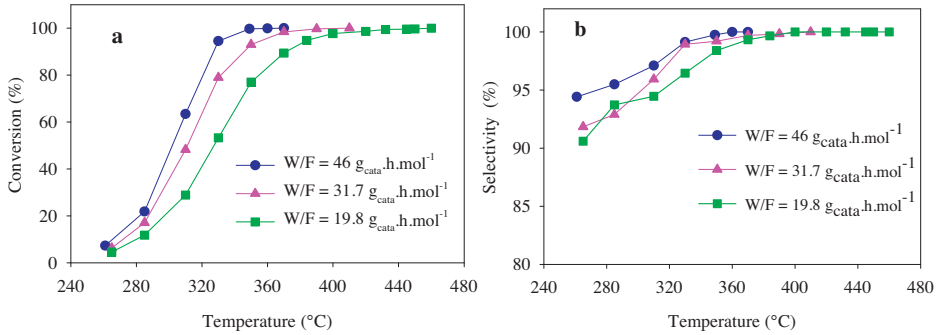

Fig. 9. Evolution of ethanol conversion (a) and ethylene selectivity (b) over $LaPO_4$-M1 catalyst at different contact times. Testing conditions: m_{cata}: 116, 80, 50 mg, N_2: 60 mL min^{-1}.

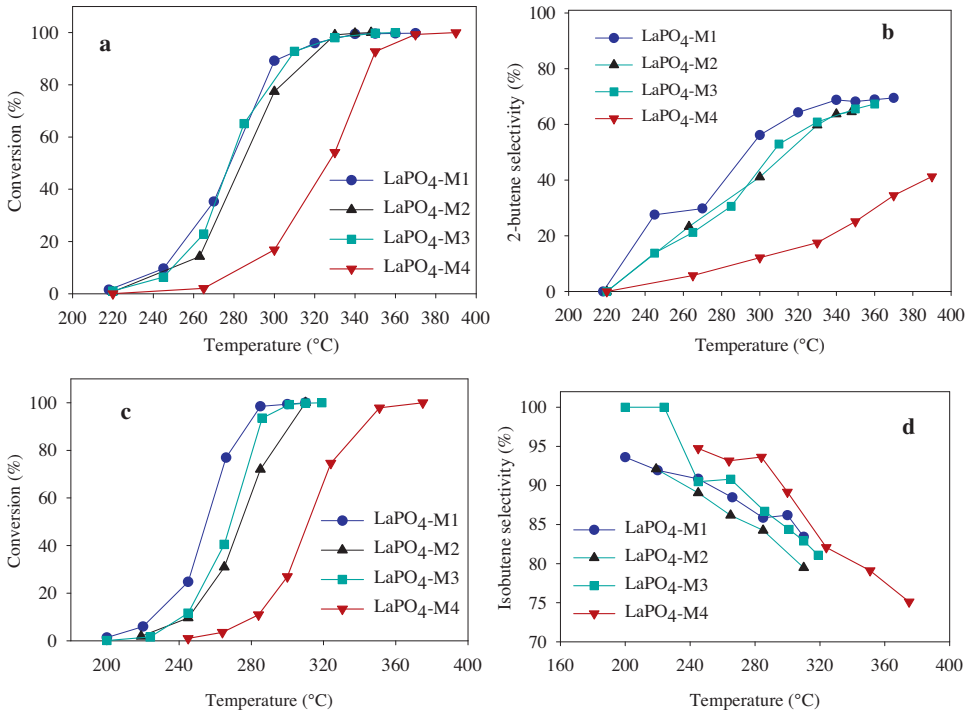

Fig. 10. Evolution of 1-butanol conversion (a) and 2-butene selectivity (b) and of isobutanol conversion (c) and selectivity to isobutene (d) as a function of temperature over the different lanthanum phosphates. Test conditions: m_{cata}: 101 mg, W/F = 31.2 g_{cata} h mol^{-1}, N_2: 100 mL min^{-1}.

Table 4
Catalytic properties of $LaPO_4$-M1 and Al_2O_3 reference in 1- and 2-propanol and 1-butanol dehydrations. Testing conditions: m_{cata}: 78 mg, W/F = 19.8 g_{cata} h mol^{-1}, N_2: 60 mL min^{-1}.

Catalyst	Alcohol	T (°C) at total conversion	Selectivity (%)			
			Propene	Propane	2-Butene	1-Butene
$LaPO_4$	1-Propanol	420	99	1		
$LaPO_4$	2-Propanol	300	100	0		
$LaPO_4$	2-Butanol	320			74	26

finer analyses of the reaction products were carried out for the dehydration of ethanol, 1-propanol and 2-butanol, in order to ascertain the presence (in ppm) of by-products or unreacted alcohols. These analyses were carried out with $LaPO_4$-M1, for the dehydration of ethanol at 460 °C, the dehydration of propanol at 420 °C, and the dehydration of 2-butanol at 320 °C. Total conversion was obtained at these temperatures. In the case of ethanol dehydration, very small peaks were detected, corresponding to acetaldehyde and diethylether. The theoretical selectivity to these products was of the order of 0.05%; in the case of propanol dehydration, propanal and propane were observed in similar quantities. Finally, in the case of 2-butanol dehydration, no compound other than 2-butanol was detected. It can thus be concluded that the conversion efficiency never reached 100%, but can nevertheless come close to 99.9%. Similarly, the selectivity to alkenes is found to be close to 99.95%, except in the case of 2-butanol for which it really attains 100%.

3.3.3. *Study of the catalysts' stability*

As it is an important factor for the evaluation of the catalysts' efficiency, the stability of their on-stream properties were studied. All of the catalysts had similar stabilities after 8 h on stream, with their conversion efficiency reduced to 99.5% and their selectivity remaining close to 100% (with the exception of $LaPO_4$-M2, which had a conversion efficiency and a selectivity of less than 98%). The stability of the best phosphate catalyst ($LaPO_4$-M1) was also compared with that of one of the best non-lanthanum-phosphate catalysts described in the literature. Very few catalysts have been tested over a long period of time and among these, the best and most stable candidate reported in the literature is HZSM-5 doped with La and P (0.5% La-2% P-HZSM-5) [11]. The $LaPO_4$-M1 catalyst was thus tested at the same WHSV (1.0 h^{-1}), but at 360 °C instead of 260 °C (Table 5). This temperature was the temperature total conversion was reached with the considered WHSV. The ethanol conversion and selectivity to ethylene over 0.5% La-2% P-HZSM-5 decreased to 97.4% and 96.4%, respectively, after 72 h.

Table 5
Comparison of ethanol conversion and selectivity to ethylene of the $LaPO_4$-M1 and 0.5% La-2% PHZSM-5 after 5 and 72 h at the same ethanol referred WHSV (1.0 h^{-1}).

Catalyst	T (°C)	5 h		72 h	
		Conv. (%)	Selec. (%)	Conv. (%)	Selec. (%)
$LaPO_4$-M1	360	100	100	99.7	99.8
0.5% La-2% P-HZSM-5 [3]	260	100	99.5	97.4	96.4

Conversely the ethanol conversion and selectivity to ethylene over the $LaPO_4$-M1 catalyst decreased only slightly, to 99.7% and 99.8%, respectively, after a similar time on stream.

4. Discussion

Different methods of preparation have been used to synthesize lanthanum orthophosphate catalysts. All of the solids were crystallized, and almost all of these were monophasic with a Rhabdophane structure. Almost all the methods of preparation allowed the catalysts to have a specific surface area greater than 120 $m^2\,g^{-1}$, which is a high value for orthophosphates. Although the porosity of the solids was not studied systematically, rather large pores (up to 14 nm) were formed and no microporosity was detected. The texture of the solids is typical of those already reported in the literature for Rhabdophane structures with small nanorods. The surface catalysts' composition is characterized by an excess of phosphorus, leading to P/La ratios ranging between 1.0 and 1.4. This phosphorus excess appears to be related to the method of preparation of the phosphate, than to its structure. Characterization of the catalysts using other techniques such as NMR, FTIR and Raman spectroscopy confirmed these results, in particular the phase purity, the nature of the structure and the presence of excess of phosphorus at the surface. They further demonstrated that the latter is related to the presence of $(H_nPO_4)^{-3+n}$ subsurface species. Acid–base properties were studied using probe molecules, with which desorption was monitored by FTIR or simply by TPD experiments. The surface acidity and basicity characteristics of the lanthanum phosphate produced using several different techniques were in agreement. Not all of the probe molecules chosen for the study were entirely suitable for the characterization the catalysts' acid–base properties. However, they were relatively easy to use and produced comparative data, which contributed to an improved understanding of the relationship between their catalytic and acid–base properties. The lanthanum phosphates were shown to have both Brønsted and Lewis acid sites. Most of the sites had a weak or medium acid strength. No very strong acid sites were revealed on these phosphates. This observation makes it more straightforward to understand the low coking ability of these catalysts. Brønsted acid sites can be related to the $((H_nPO_4)^{-3+n})$ species detected at the surface of the solids, and Lewis acid sites can be related to rare earth cations. The catalysts' acidic properties thus depend on their surface composition, which is itself related to the method of preparation. Another important result is that the lanthanum phosphate catalysts have very few basic sites with weak or moderate strength. As in the case of the acid sites, the number of basic sites also appears to depend on the method of preparation.

Before proposing an interpretation of the correlation observed between the acid–base and the catalytic properties of these catalysts, it is important to recall some elementary considerations related to the mechanisms involved in the dehydration reaction. With the E_1 mechanism, the first dehydration step corresponds to the formation of a carbenium ion, by abstraction of an OH group. This mechanism occurs with acidic catalysts, for a relatively large range of acid strengths. The acidic center may be of either the Brønsted or the Lewis type. In the former case, isomerization occurs at the carbenium ion stage, and the formation of 2-butene isomers from 1-butanol is indicative of the E_1 mechanism. With the E_2 mechanism, a proton and a hydroxyl group are eliminated from the alcohols in a concerted manner, without the formation of ionic intermediates. Both acidic and basic centers are directly involved in this mechanism. A lack of 2-butene, or the exclusive formation of 1-butene from 1-butanol, is indicative of the E_2 mechanism. From 2-butanol, preferential formation of 2-butene (Saytzev orientation) is observed. It was shown many years ago by Knözinger et al. that

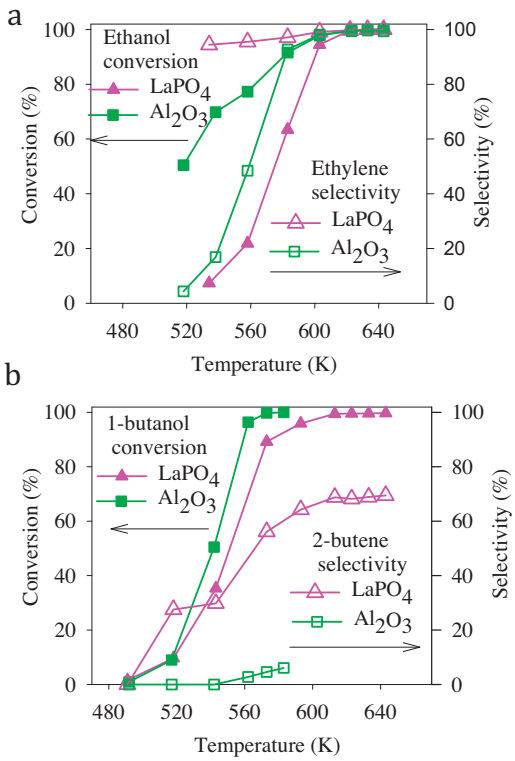

Fig. 11. Comparison of the catalytic properties of Al_2O_3 and $LaPO_4$-M1: (a) in ethanol dehydration (test conditions: m_{cata}: 116 mg, W/F = 46 g_{cata} h mol^{-1}, N_2: 60 mL min^{-1}) and (b) in 1-butanol dehydration (test conditions: m_{cata}: 101 mg, W/F = 31.2 g_{cata} h mol^{-1}, N_2: 100 mL min^{-1}).

this type of mechanism typically occurs on Al_2O_3 [41]. It was thus of interest to compare the catalytic properties of $LaPO_4$-M1 with those of anAl_2O_3 reference catalyst (Fig. 11). The catalytic properties of these two solids were comparable in the dehydration of ethanol, although Al_2O_3 appeared to be more active at low temperatures and slightly less selective (98.8%) to ethylene than $LaPO_4$-M1 at total conversion. However, the catalytic properties in the dehydration of 1-butanol were very different, since Al_2O_3 appeared to be poorly selective to 2-butene. In the E_{1cB} mechanism, the first step corresponds to the formation of carbanion: a C—H bond is loosened or broken in the first step. This mechanism occurs with strongly basic catalysts such as alkaline earth oxides [42]. If a dehydrogenation reaction is observed in addition to dehydration, this provides a good indication of the E_{1cB} mechanism. In the case of dehydrogenation the H^- is abstracted from the anion by the surface, whereas OH^- is abstracted in the case of dehydration. In the case of 2-butanol dehydration, a high selectivity to 1-butene (Hofmann orientation) is observed, whereas the E_1 and E_2 mechanisms produce mainly 2-butene. The abstraction of protons by basic sites to form anionic species is the key step in this mechanism which has been reported to occur on catalysts such as ZrO_2 [43].

It is important to note that these different mechanisms can occur simultaneously and to different degrees on the same catalyst, depending on the distribution of the acid and basic sites. The type of mechanism, as well as the sites' populations, can also vary as a function of the reaction temperature. This also depends on the types of dehydrated alcohol involved (primary, secondary or tertiary). Furthermore, it has been reported that some compensation effects may also occur in the case of dehydration on oxide catalysts. As a consequence of the aforementioned considerations, it is often difficult to study and compare the catalytic properties of different solids, with respect to a given reaction mechanism.

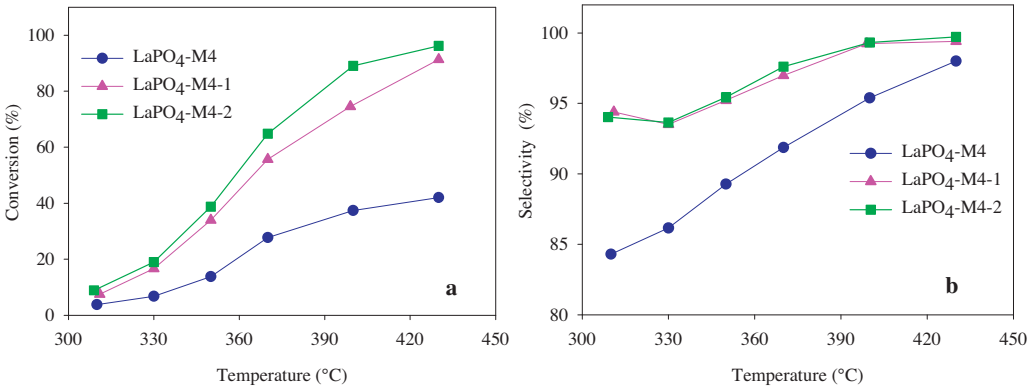

Fig. 12. Evolution of 1-butanol conversion (a) and selectivity to 2-butene (b) on $LaPO_4$-M4 prepared with different P/La ratios. Testing conditions: m_{cata}: 101 mg, W/F = 31.2 g_{cata} h mol^{-1}, N_2: 100 mL min^{-1}; (1) and (2) correspond to $LaPO_4$-M4-1 and -2 respectively.

The present study of the dehydration of 1-butanol revealing a very high selectivity to 2-butene over lanthanum orthophosphate contributes to the hypothesis that these catalysts are involved mainly with the E_1 mechanism. Although the presence of the E_2 mechanism may be considered in particular at low temperature where the selectivity to 2-butene is lower, that of the E_{1cB} mechanism can be discarded in view of the catalytic data and because of the small number of only weak basic sites detected.

The prevalence of the E_1 mechanism is also confirmed by the absence of isobutene produced either from 1-butanol or 2-butanol dehydration that can only be formed from their skeletal isomerization [44,45]. Furthermore the effect of water has been studied by adding 12.5% of water to the gas feeds and no effect was evidenced either on the conversion, nor the selectivity, which tend to show that no reverse reaction takes place at the considered reaction temperature that could have distorted the interpretation of the results. The later result can certainly be explained because butenes cannot compete with butanols for adsorption on the only weak or moderately strong acid sites. Such prevalence of the E_1 mechanism has already been evidenced on phosphates in the case of BPO_4 [47]. With that respect $LaPO_4$ should resemble BPO_4 but with the advantage of not been partly soluble in water.

The differences observed between the catalytic properties of the lanthanum phosphate-based catalysts remains to be explained. When the catalytic properties of $LaPO_4$-M1 and $LaPO_4$-M4 are compared in terms of the dehydration of 1-butanol, the role of the nature of the sites involved in this reaction can be better understood. $LaPO_4$-M1 is more active than M4, and considerably more selective to the formation of 2-butene. Besides the fact that they were prepared using different methods, $LaPO_4$-M1 had a greater surface P/La ratio than $LaPO_4$-M4. When $LaPO_4$-M4 samples were prepared with an excess of phosphorus (M4-1 and M4-2) the solids exhibited higher P/La surface ratios. Testing of these catalysts in the dehydration of 1-butanol clearly showed that both their activity and their selectivity to 2-butene were significantly improved (Fig. 12). This indicates that an excess of phosphorus, which creates Brønsted acid sites, leads to the formation of catalytic sites, which are active and selective for 2-butene dehydration. Moreover, the acidity characterization of the $LaPO_4$-M1 and M4 samples indicates that $LaPO_4$-M4 has a greater number of Lewis acid sites and a considerably smaller number of Brønsted acid sites than M1. It can thus be concluded that both Lewis and Brønsted acid sites are active for 1-butanol dehydration, although Brønsted acid sites are more active than Lewis acid sites. Selectivity also appears to be influenced by the nature of the sites.

The Lewis acid sites of lanthanide phosphates may also be involved in an E_2 mechanism, whereas the Brønsted acid sites on lanthanum phosphates are involved in the E_1 mechanism. The less active and less selective catalysts thus have a higher Lewis acid site density, and a lower Brønsted acid site density than the others. $LaPO_4$-M2, which exhibits an activity and a selectivity lying between the values found for $LaPO_4$-M1 and $LaPO_4$-M4 in the dehydration of 2-butene, also has an intermediate P/La surface ratio and an intermediate number of Brønsted acid sites. Indeed, the level of activity in the different reactions can be systematically ranked in the same order: M1 > M3 > M2 > M4. The P/La surface ratios are ranked in the same order. This can be more easily understood when the rate of ethanol conversion at 350 °C is plotted as a function of the surface P/La ratio (Fig. 13). This figure shows that the conversion rate increases almost linearly with the P/La ratio. Interestingly, the M4 catalysts prepared with a phosphorus excess (M4-1 and M4-2) follow this general trend, but with a significant gap. The ^{31}P NMN CP-MAS spectrum of $LaPO_4$-M4-2 reveals a small peak at 10.8 ppm, attributed to the presence of polyphosphates. This shows that not only the quantity, but also the dispersion of subsurface phosphoric species plays a role. The latter appeared to depend on the method of preparation, and attempts to boost the surface P/La ratio did not systematically lead to more efficient catalysts, since they also led to the formation of species, which were different from the most active species ($(H_nPO_4)^{-3+n}$) and appeared to be less efficient. It should be noted that a dependence on the rate of ethanol conversion, expressed in mmol of ethanol per g per second as a function of the acidity, expressed in mmol of sites per g of catalyst, has been reported by Ramesh et al. [14].

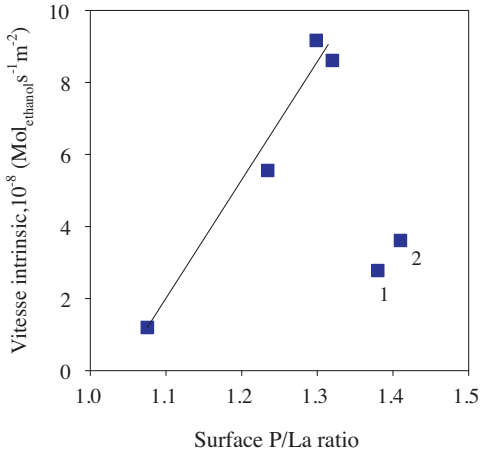

Fig. 13. Variation of the initial rate of ethanol conversion as a function of the surface P/La ratio.

The case of $LaPO_4$-M3 is more complex than that of the other phosphates, since ammonium cations were detected on its surface. These cations were eliminated when it was pre-treated under vacuum at a high temperature to determine its acid–base properties. It thus exhibited a higher Brønsted site density than that involved in the catalytic reaction during testing at 285 °C. However, at higher temperatures the activity of this catalyst appeared to be as high as that of $LaPO_4$-M1 (Fig. 13).

The conclusions reached in the preceding discussion for the case of ethanol dehydration are valid for 1-butanol dehydration. However, in view of the NH_3-TPD data, the results of the catalytic testing indicate that strong acid sites are required for ethanol dehydration on lanthanum phosphates, whereas not only strong acid sites, but also weak and moderately weak acid sites are active for 1-butanol dehydration.

The results obtained for the dehydration of 1- and 2-propanol indicate that propylene could be formed more efficiently from 1-propanol by an E_2 mechanism such as that observed on Al_2O_3, than by an E_1 mechanism such as that observed on lanthanum phosphate, whereas this alkene appeared to be similarly formed from 2-propanol by either the E_1 or the E_2 mechanism [46]. It is interesting to note that in a previous study, similar conclusions were reached concerning the dehydration mechanisms of the acid catalyzed dehydration of 1-and 2-propanol in hot compressed liquid water [48]. The latter paper also explains why 2-propanol, which is extensively used to probe the acidity of catalysts, may sometimes lead to questionable results concerning a catalyst's acidity.

The E_2 mechanism could take place on lanthanum phosphates on lanthanum phosphates such as $LaPO_4$-M4, having a high number of low strength Lewis acid sites and a low number of Brønsted sites. However, these catalysts did not appear to be efficient; the presence of Lewis acid sites was insufficient, such that basic sites could also be needed. In that respect all lanthanum phosphate catalysts have a singularly low number of weak basic vs acid sites, when compared to most other dehydration catalysts described in the literature.

Before trying to understand the influence of the catalysts' structure, it was important to verify that the testing did not lead to any change in this structure. X-ray diffraction patterns of the solids were recorded after testing. No phase transformation was observed, except when the catalysts were tested at a temperature above 460 °C. In this case, very small peaks corresponding to the Monazite structure were observed, indicating a partial transformation of the Rhabdophane structure. There are two parameters determining the texture of the solid, which may have a significant influence on its catalytic properties during heterogeneous catalysis: the solid's porosity and the shape of its particles. Tsukuda et al. [49] have shown that the pore diameter of a dehydration catalyst has an influence on its stability. They showed that this should be chosen to be close to 10 nm, in order to obtain the best performance from a given catalyst. This was also confirmed by Znaiguia et al. [50] in the case of glycerol dehydration on tungstated zirconias. Most of the catalysts had pore sizes ranging from 8 to 12 nm ($LaPO_4$-M1, M3 and M4), which was positive. Only the $LaPO_4$-M2 catalyst had smaller pore sizes close to 5 nm. A comparison of the stability of the catalytic properties of $LaPO_4$-M2 and $LaPO_4$-M1, as a function of time spent on stream, showed that after 8 h the deactivation of ethanol dehydration on $LaPO_4$-M2 was greater than that on $LaPO_4$-M1. This appears to confirm the influence of pore size on the catalyst's stability.

Concerning the shape of a catalyst's particles, transmission electron microscopy analysis shows that these were nanorods with comparable lengths and thicknesses. Again only the $LaPO_4$-M2 catalyst prepared by mecano-synthesis had a different morphology with particles having unspecific shapes. No specific influence on the catalytic properties could be clearly related to the particles shape, and it is not possible to conclude as to whether the active sites are not situated on any specific faces, or at the ends of the nanorods.

5. Conclusion

The high efficiency of lanthanum orthophosphate in the dehydration of numerous mono-alcohols has been confirmed [14]. A combination of different preparation techniques (M1 and M4) and the best catalyst compositions allowed the catalysts to be optimized for several important reactions. The choice of method of preparation has a significant impact on catalytic performance, since it influences the shape of the particles and the catalysts' porosity, structure and surface composition. Although the shape of the particles does not appear to play an important role, their porosity has been shown to influence the catalysts' stability. Some of the results obtained in this study confirm those already observed with other dehydration catalysts, namely that pore sizes of 10 nm or more are needed to slow down the deactivation attributed to the irreversible adsorption of oligomer species and/or to the formation of coke. Regeneration of the catalyst by means of a simple heat treatment under air has been shown to be efficient. The most significant parameter appears to be the catalyst's surface composition (P/La ratio), since this has a direct impact on its acidity.

Various techniques allowed the acid–base properties of the catalysts to be correlated with their catalytic properties. The resulting correlations did not differ significantly from one alcohol to another. All of the solids have Brønsted and Lewis acid sites with broad strength distributions but with mainly weak and moderated acid strengths and only low quantities of weak basic sites. These acid–base properties resulted in the prevalence of the E_1-type mechanism for 1-butanol dehydration as confirmed by the high selectivity to 2-butene. The Brønsted acid sites appeared to be more active and selective than the Lewis acid sites. Their presence has been attributed mainly to an excess of phosphorus at the surface of the phosphates. This was detected by XPS revealing surface P/La ratios between 1 and 1.4. From results of other spectroscopic techniques this excess has been attributed to $(H_nPO_4)^{-3+n}$ species, which are formed naturally by the charge balance process during the preparation of the catalysts. The excess phosphorus content thus depends on the preparation method. Attempts to increase this content were successful but also led to the formation of polyphosphates species.

Lewis acid sites, which could be related to incomplete surface coordination of the lanthanum cations, may intervene either directly, in the form of active Lewis acid sites or indirectly after conversion to Brønsted acid sites under catalytic reaction conditions in the presence of large quantities of water. However the direct relationship observed between the surface excess of phosphorus led to the conclusion that these sites could be considerably less active. The extremely high selectivity of the lanthanum phosphates may be related to the uniformity of the active acid sites ($(H_nPO_4)^{-3+n}$ species) which function according to a mainly E_1-type mechanism and to the nearly total absence or very low strength of basic sites. Experiments with isotopically labeled alcohols would be needed in order to confirm the nature of the reaction mechanism for each alcohol and to calculate the percentage of E_1 versus E_2 mechanism.

Finally it should be emphasized that apart from their interesting intrinsic activity and ultra-selectivity, the lanthanum phosphates tested in this study were highly stable as a function of time on stream and could be easily regenerated by means of heat treatment under air, thus making them useful for industrial applications. The absence of very strong acid sites, which are preferential sites for the formation of coke, could explain both their high selectivity and relative stability. Furthermore the present study has shown that the broad distribution of acid sites on these catalysts, could allow them to be used for the dehydration of versatile alcohols.

Acknowledgments

ADISSEO is thankfully acknowledged for financial support. The authors would like to thank M. Aouine who provided help in the recording and analysis of HRTEM data.

References

[1] A. Chauvel, G. Lefebvre, L. Catex, Procédés de pétrochimie, tome 1, Ed Technip, Paris, 1985.
[2] A. Morschbacker, J. Macromol. Sci. Part C: Polym. Rev. 49 (2009) 79–84.
[3] O. Winter, E. Ming-Teck, Hydrocarb. Process. 11 (1976) 125–133.
[4] C.B. Phillips, R. Datta, Ind. Eng. Chem. Res. 36 (1997) 4466–4475.
[5] T.M. Nguyen, R.L.V. Mao, Appl. Catal. 58 (1990) 119–129.
[6] X. Zhang, R. Wang, X. Yang, F. Zhang, Microporous Mesoporous Mater. 116 (2008) 210–215.
[7] K. Ramesh, L.M. Hui, Y.F. Han, A. Borgna, Catal. Commun. 10 (2009) 567–571.
[8] D.S. Zhang, R.J. Wang, X. Yang, Catal. Lett. 124 (2008) 384–391.
[9] R.L.V. Mao, St-Laurent, US Patent 4,873,392 (1989).
[10] J. Ouyang, F.X. Kong, G.D. Su, Y.C. Hu, Q.L. Song, Catal. Lett. 132 (2009) 64–74.
[11] N. Zhan, Y. Hu, H. Li, D. Yu, Y. Han, H. Huang, Catal. Commun. 11 (2010) 633–637.
[12] P. Brandao, A. Philippou, J. Rocha, M. Anderson, Catal. Lett. 80 (2002) 99–102.
[13] L. Matachowski, M. Zimowska, D. Mucha, T. Machej, Appl. Catal. B: Environ. 123–124 (2012) 448–456.
[14] K. Ramesh, J.E. Zheng, E. Goh, Y. Ling, Y.F. Han, A. Borgna, J. Phys. Chem. C 113 (2009) 16530–16537.
[15] K. Ramesh, Y.L.E. Goh, C.G. Gwie, C. Jie, T.J. White, A. Borgna, J. Porous Mater. 19 (2012) 423–431.
[16] J.M.M. Millet, T.T.N. Nguyen, V. Belliere-Baca, P. Rey, Fr Patent 1350926 (2013).
[17] M. Anbia, M.K. Rofouel, S.W. Husain, Chin. J. Chem. 24 (2006) 1026–1030.
[18] J.A. Diaz-Guillen, A.F. Fuentes, S. Gallini, M.T. Colomer, J. Alloys Compd. 427 (2007) 87–93.
[19] K. Rajesh, P. Shajesh, O. Seidel, P. Mukundan, K.G.K. Warrier, Adv. Funct. Mater. 17 (2007) 1682–1690.
[20] J.M. Cowlick, J.C. Wheatley, W.L. Kehl, J. Catal. 56 (1970) 185–194.
[21] C.R. Patra, G. Alexandra, S. Patra, D.S. Jacob, A. Gedanken, A. Landau, Y. Gofer, New J. Chem. 29 (2005) 733–739.
[22] H. Assaaoudi, A. Ennaciri, A. Rulmont, Vib. Spectrosc. 25 (2001) 81–90.
[23] G.M. Begun, G.W. Beall, L.A. Boatner, W.J. Gregor, J. Raman Spectrosc. 11 (1981) 273–278.
[24] O.P. Ivanova, A.V. Naumkin, L.A. Vasilyev, Vacuum 47 (1996) 67–71.
[25] S. Jørgensen, J.A. Horst, O. Dyrlie, Y. Larring, H. Raeder, T. Norby, Surf. Interface Anal. 34 (2002) 306–310.
[26] P. Bonnet, J.M.M. Millet, C. Leclercq, J.C. Védrine, J. Catal. 158 (1996) 128–141.
[27] W.P.A. Jansen, M. Ruitenbeek, A.W. Denier van der Gon, J.W. Geus, H.H. Brongersma, J. Catal. 196 (2000) 379–387.
[28] I.C. Marcu, I. Sandulescu, J.M.M. Millet, Appl. Catal. A: Gen. 227 (2002) 309–320.
[29] G. Niaura, A.K. Gaigalas, V.L. Vilker, J. Phys. Chem. B 101 (1997) 9250–9262.
[30] S.B. Moussa, S. Ventemillas, A. Cabeza, E. Gutierrez-Puebla, J. Sanza, J. Solid State Chem. 177 (2004) 2129–2137.
[31] D.D. Perrin, B. Dempey, E.P. Sejeant, pK, Prediction for Organic Acids and Bases, Chapman and Hall, London, 1981.
[32] G. Busca, Catal. Today 41 (1998) 191–206.
[33] M.A.A. Aramendía, V. Borau, C. Jiménez, J.M.A. Marinas, F.J. Romero, J. Colloid Interface Sci. 217 (1999) 288–299.
[34] B. Chakraborty, B. Viswanathan, Catal. Today 49 (1999) 253–260.
[35] O.V. Manoilova, S.G. Podkolzin, B. Tope, J.A. Lercher, E.E. Stangland, J.-M. Goupil, B.M. Weckhuysen, J. Phys. Chem. B 108 (2004) 15770–15781.
[36] E.R.A. Matulewicz, F.P.J.M. Kerkhof, J.A. Moulijn, H.J. Reitsma, J. Colloid Interface Sci. 77 (1980) 110–119.
[37] C. Flego, I. Kiricsi, C. Perego, G. Bellussi, Catal. Lett. 35 (1995) 125–133.
[38] P.A. Jacobs, C.F. Heylen, J. Catal. 34 (1974) 267–274.
[39] H.J. Freund, M.W. Roberts, Surf. Sci. Rep. 25 (1996) 225–273.
[40] M. Melle-Franco, G. Pacchioni, A.V. Chadwick, Surf. Sci. 478 (2001) 25–34.
[41] H. Knözinger, H. Bull, K. Kochloefl, J. Catal. 17 (1970) 252–263.
[42] S. Bernal, J.M. Trillo, J. Catal. 66 (1980) 184–190.
[43] T. Yamaguchi, H. Sasaki, K. Tanabe, Chem. Lett. 7 (1976) 677–678.
[44] K. Thomke, J. Catal. 44 (1976) 339–344.
[45] O. Olaofe, P.L. Yue, Collect. Czech. Chem. Commun. 50 (1985) 1834–1841.
[46] T.T.N. Nguyen, (PhD thesis), Development and study of new catalysts for C_2-C_4 alcohols dehydration, Claude-Bernard University Lyon 1 143, 2013.
[47] K. Thomke, H. Noller, Proceedings of the Fifth International Congress on Catalysis, Florida, 1972, pp. 1182–1186.
[48] M.J. Antal Jr., M. Carlsson, X. Xu, D.G.M. Anderson, Ind. Eng. Chem. Res. 37 (1998) 3820–3829.
[49] E. Tsukuda, S. Sato, R. Takahashi, T. Sodesawa, Catal. Commun. 8 (2007) 1349–1353.
[50] R. Znaiguia, L. Brandhorst, N. Christin, V. Bellière Baca, P. Rey, J.M.M. Millet, S. Loridant, Microporous Mesoporous Mater. 196 (2014) 97–103.